Available online at www.sciencedirect.com
SCIENCE DIRECT
Journal of Molecular Catalysis A: Chemical 253 (2006) 52–61
JOURNAL OF MOLECULAR CATALYSIS A: CHEMICAL
www.elsevier.com/locate/molcata

Counterion and additive effects on ethylene coordination and insertion in metallocene catalyst

P.G. Belelli, N.J. Castellani *

Grupo de Materiales y Sistemas Catalíticos, Departamento de Física, UNS, Avenida Alem 1253, 8000 Bahía Blanca, Argentina

Received 5 December 2005; received in revised form 2 March 2006; accepted 3 March 2006
Available online 18 April 2006

Abstract

A theoretical analysis of coordination and insertion of the ethylene molecule on different metallocenic active sites was performed. The sites were modelled as ionic-pairs where the counterion is close to the cation. The steps going from the isolated species ionic-pairs and the monomer to the new propyl group linked to the ionic-pair were calculated and analyzed. The influence of the counterion on the energy barrier that the olefin must overcome for its coordination and insertion into the $Zr{-}C_{CH_3}$ bond was considered. The energy barrier is decreased by the inclusion of an $AlCl_3$ additive. As an additional study, the presence of a second ethylene molecule in the neighborhood of the active site was evaluated. This situation reduces the maximum energy and improves the stability of the final propyl ionic-pair.

Keywords: Metallocene polymerization; Counterion effect; $AlCl_3$ additive; DFT calculations

1. Introduction

Catalysts based on metallocene complexes have been the subject of intensive studies in the last years due to their ability to polymerize olefins [1]. These complexes are only active after treatment with Lewis acidic co-catalysts. Since the discovery of the most powerful activator, methylaluminoxane (MAO), the polymerization field has been increasing noticeably. It is generally assumed that MAO works in two different steps: a fast ligand exchange reaction with the metallocene dichloride to form the methyl metallocene, and in another step, Cl abstraction from the metallocene. In this way, the metallocene cation and the $MAOCl^-$ counterion are produced. Nevertheless, other functions could be attributed to this co-catalyst. Many reports suggest that the properties of metallocene catalysts are intimately related to the strength of the cation–anion ion pair [2]. At present, the presence of counterion in the active sites during the olefin coordination and insertion is widely recognized. The nature of the co-catalyst with its forthcoming sterical and electronic effects on the catalyst should have a critical influence on the catalytic reaction.

In the last decade, the number of theoretical studies on metallocene catalysts has been increasing. There are many computational investigations which consider an isolated cation as a model of active site [3–5]. On the other hand, there are few papers where the metallocenic catalysts include the co-catalyst, being $B(C_6F_5)_3$ [6–8] the most explored. Studies of the olefin coordination and insertion processes with an isolated cation model predicted energies lower than for the cation and monomer separated [9–11].

In our previous works, the Cp_2ZrCl_2/MAO (Cp denotes η_5-C_5H_5) system characterizing two types of active sites was theoretically considered [12]. The co-catalyst was modelled as the most reactive fraction of a three-dimensional cage structure with four-coordinated aluminium centers bridged by three-coordinate oxygen atoms [13]. In a later work, the role of a third component in the catalytic system was taken into account: the Lewis acid $AlCl_3$ was included to interact with the co-catalyst [14]. The results indicated that the additive favoured the active site formation provoking modifications on its geometry and electronic structure.

The most widely accepted mechanism for olefin polymerization on Ziegler-Natta and metallocene catalysts is the Cossee-Arlman mechanism [10,15]. It consists mainly of two sequential processes: (1) olefin coordination to the vacant site of the metal (M) atom and (2) olefin insertion into the $Zr{-}C_{CH_3}$ bond through

* Corresponding author. Tel.: +54 291 459 5141; fax: +54 291 459 5142.
E-mail addresses: pbelelli@plapiqui.edu.ar (P.G. Belelli), castella@criba.edu.ar (N.J. Castellani).

1381-1169/$ – see front matter © 2006 Elsevier B.V. All rights reserved.
doi:10.1016/j.molcata.2006.03.004

a four-member transition state. The growing polymer changes its position during successive steps.

The aim of this paper is to study the ethylene coordination and insertion on the metallocenic active sites modelled as ionic-pairs, following the inherent geometric, energetic and electronic charge variations. In addition, the influence of $AlCl_3$ as an additive and the behaviour of active site at the presence of two ethylene molecules were also considered.

2. Theoretical method and models

The theoretical calculations were performed within the Density Functional Theory formalism (DFT), using the hybrid functional B3LYP [16,17] which corresponds to Becke's three-parameter hybrid exchange and to the Lee, Yang, and Parr's correlation functional. The molecular orbitals were constructed with a Gaussian 3-21G** basis set, which includes polarization p-type functions on hydrogen atoms and d-type functions on C, O, Al and Cl atoms. Previous results performed with the 6-31G** basis set gave reaction energy values only 10% lower than those corresponding to the 3-21G** basis set [14]. For the Zr atom, an effective core potential (ECP) basis set was used to describe the inner and valence orbitals. Here, the LanL2DZ ECP basis set (Los Alamos Effective Core Potential plus Double Z) has been employed [18]. This ECP has been successful to study Zr-organometallics [19]. All the calculations were performed using the GAUSSIAN 03 program [20].

Molecular and atomic charges, electron transfers and molecular orbital occupations were obtained with the Natural Bond Orbital (NBO) population analysis [21]. Within this approach localized orbitals with occupation numbers close to two correspond either to core, bonds and/or lone pairs, localized orbitals with occupation number notably smaller than one, to antibonding and Rydberg orbitals. Their respective occupation numbers are given by the density-matrix element as calculated in the NBO basis. Since the Fock-like matrix is not diagonal in the NBO basis, it is also possible to evaluate, by means of the second order perturbation theory, the delocalization energy, $\Delta E^{(2)}$, associated to the charge delocalization from a highly occupied orbital.

The energy balance (ΔE) for each considered step was calculated as the difference between the energy of the ionic-pair with the ethylene molecule and the sum of energies corresponding to

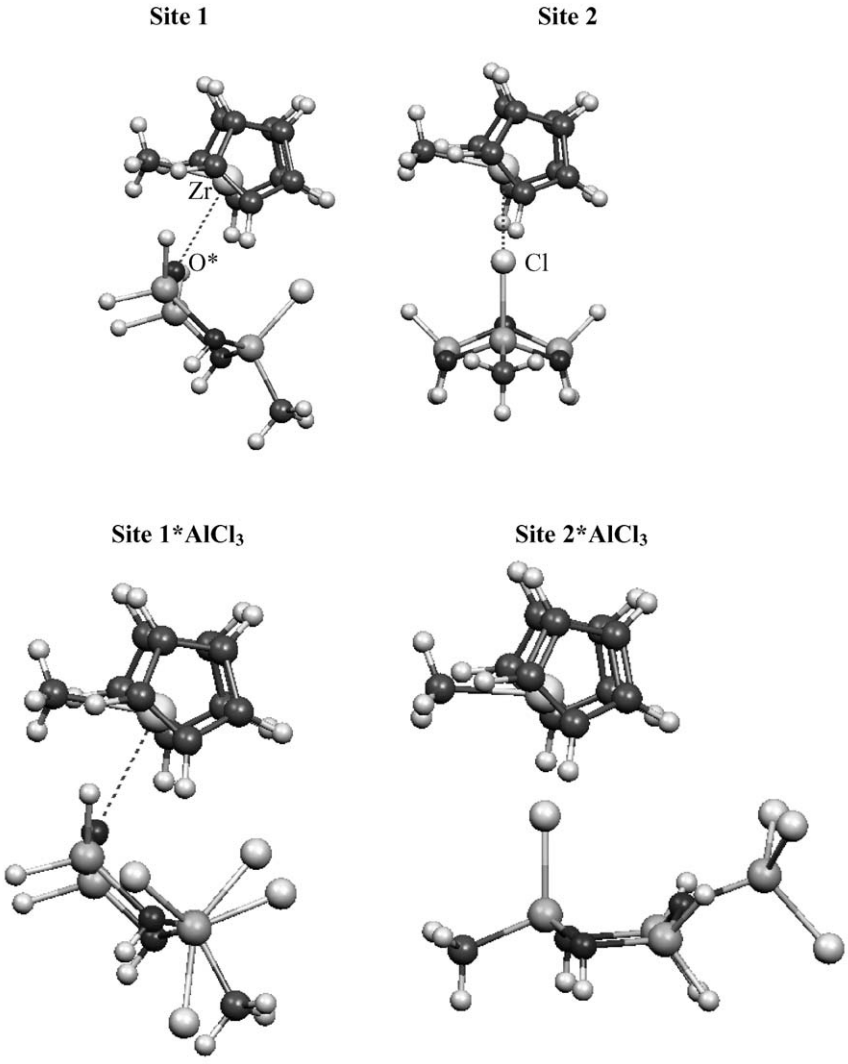

Fig. 1. Optimized models of Site 1 and Site 2 with and without $AlCl_3$ additive.

the free ionic-pair and the ethylene molecule. A negative value indicates an exothermic process. Reported energies are not corrected for either thermal or zero-point energy. The coordination plus insertion reaction of the ethylene molecule in the active site, and its total energy balance ΔE are expressed by the following equations:

$$Cp_2ZrCH_3^+ \cdots MAO\text{–}Cl^- + CH_2{=}CH_2 \rightarrow Cp_2ZrCH_3^+ \cdots MAO\text{–}Cl^- // CH_2{=}CH_2 \quad \text{(E1)}$$

$$\Delta E = E_T(Cp_2ZrCH_3^+ \cdots MAO\text{–}Cl^- // CH_2{=}CH_2) - E_T(Cp_2ZrCH_3^+ \cdots MAO\text{–}Cl^-) - E_T(CH_2{=}CH_2) \quad \text{(E2)}$$

During the coordination and insertion processes the C_2–C_{CH_3} distance was progressively shortened and at the same time a geometry optimization was carried out with C_s symmetry constraint. The geometry optimization was based on the Berny algorithm [22]. Each reaction step can correspond to a local minimum, maximum or saddle point on a certain curve of the multidimensional potential energy surface. To define the character of such stationary states, a calculation of Hessian eigenvalues without C_s symmetry constraint was performed.

The geometries of the active sites with and without $AlCl_3$ additive were previously determined [12]. They are represented by ionic-pairs, specifically the metallocenic $Cp_2ZrCH_3^+$ cation and the $MAOCl^-$ counterion. For MAO co-catalyst a model developed earlier consisting by a fraction of a MAO cage was adopted. The size consistency of energies and geometries for this model was verified comparing with a greater portion of the MAO cage [12]. Two different geometries for active sites were considered. Site 1 corresponds to the closest bond connecting the Zr atom of the cation and the bridge oxygen atoms (O*) of the counterion. Site 2 with a more open geometry concerns to the interaction between the Zr atom and the Cl atom of the counterion. The $AlCl_3$ additive has an indirect effect on the cation through the counterion. The corresponding geometries are depicted in Fig. 1.

3. Results and discussion

3.1. Study with one ethylene molecule

For the present study different steps were analyzed, taking into account the coordination and insertion processes of the ethylene molecule. In Fig. 2, the energetic profile and the optimized geometries of Site 1 are exhibited. The obtained results indicate that an energetic requirement (of ~6.7 kcal/mol) for the initial coordination of ethylene is necessary, a Zr-coordinated complex being formed (Step 1). The later insertion of the olefin on the Zr–C_{CH_3} bond requires a certain degree of deformation with a greater consumption of energy (of ~7.7 kcal/mol). A four-member state (Step 2), constituted by the Zr atom, the C atom of the methyl group and the two C atoms of the ethylene, is created. In the following step the monomer insertion into the Zr–C_{CH_3} bond takes place (Step 3) through the liberation of a non-negligible amount of energy (of ~3.6 kcal/mol). An

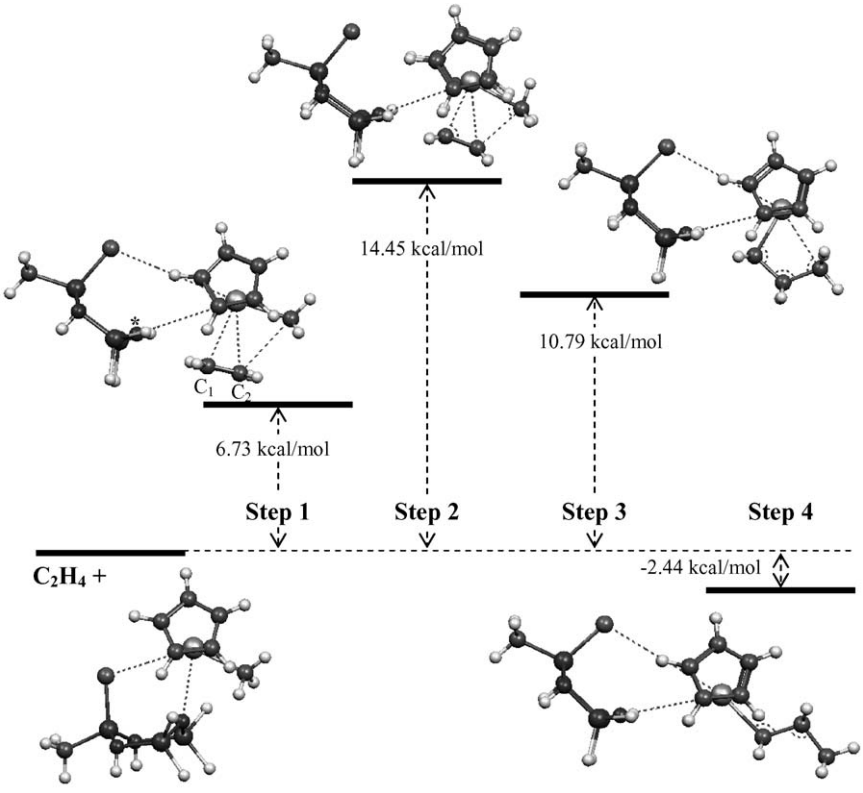

Fig. 2. Energy profile and optimized geometries for ethylene activation and insertion into the Site 1. The zero reference in the energy scale is for the isolated reagents.

intermediate complex with a propyl group is formed, having a relatively high positive ΔE compared to the reactants. Finally, a subsequent relaxation of propyl chain (Step 4) produces a further and relevant energy decrease of the system (by ~13.2 kcal/mol). In this final step, the propyl ionic-pair attains a slightly lower energy than the active site without olefin ($\Delta E \sim 2.4$ kcal/mol). Looking at the Hessian eigenvalues, it was observed that the Steps 1, 3 and 4 correspond to local minima and the Step 2 to a maximum of the potential energy surface.

The complex formation and insertion of the ethylene molecule was also studied in other situations: Site 1 with $AlCl_3$, Site 2 and Site 2 with $AlCl_3$, whose energy profiles and geometries are shown in Figs. 3–5, respectively. Regarding the Site 2, we notice that the Zr-coordinated complex and maximum energies are approximately 3.1 and 3.5 kcal/mol greater, respectively, than the corresponding steps of Site 1. After reaching the four-membered state, the formed propyl group is located far away with respect to the counterion. This situation is energetically favourable, giving for the complex intermediate of Step 3 an exothermic ΔE value (of ~6 kcal/mol). It could be explained by the better orbital overlap of the Zr atom and the C atom from the propyl group. Finally, at Step 4 a large stabilization was obtained though the relaxation of propyl chain, lowering the energy by ~15.4 kcal/mol, as it was observed in Site 1.

It is noteworthy to compare the energy profile predicted for our analyzed system with that obtained by Zurek and Ziegler for the insertion of ethylene into the $[Cp_2ZrMe]^+[AlMe_3MeMAO]^-$ ionic-pair using other model of MAO [8]. While the insertion barrier calculated by these authors reaches 18.5–23.8 kcal/mol, our corresponding results are of 14.4 (Site 1) to 18.0 kcal/mol (Site 2). Moreover, their reported Zr-coordinated complex has the 91–95% of this barrier, while in our calculations they are of 47 (Site 1) to 55% (Site 2). On the other hand, no propyl complexes were reported in Ref. [8]. Moreover, the energy profiles obtained here are also similar to those found in the open literature for other metallocenic systems [23]. Taking into account our experience of the influence of solvent on metallocenic catalytic systems, it is likely that the energy profile would be more smoothly, nevertheless the qualitative results would be maintained [24].

The $AlCl_3$ addition decreases the general energy profiles for the polymerization on both active sites, decreasing the energy barrier by ~2.5 kcal/mol at Site 1 and by ~5 kcal/mol at Site 2. Very recently, a theoretical analysis of the $AlCl_3$ modified catalytic system has been realized [12,14,24]. However, the role of the additive on the metallocenic site during the polymerization mechanism is considered theoretically here for the first time. From the ionic-pair formation to the polymerization reaction, the additive improves each step in the catalytic process. These results are in agreement with previous experimental work, where the $AlCl_3$ addition produces an increase in the catalyst performance [25,26].

The geometric changes of the both active sites with and without additive are shown in Table 1. In Step 1, the $Zr{-}C_{CH_3}$

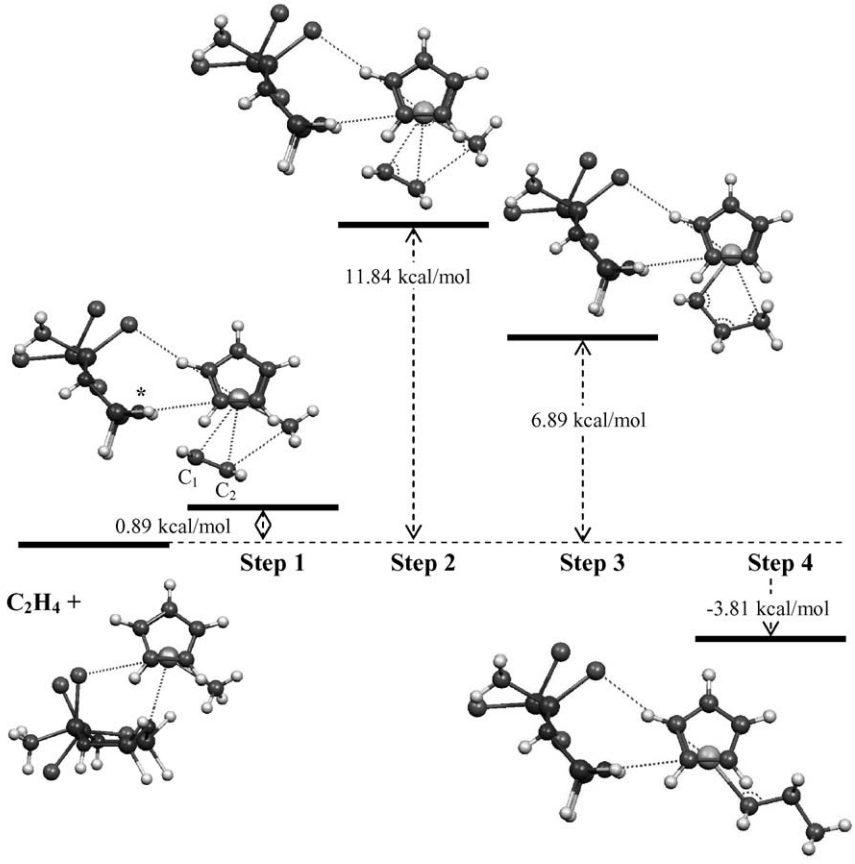

Fig. 3. Energy profile and optimized geometries for the ethylene activation and insertion into the Site 1 with $AlCl_3$.

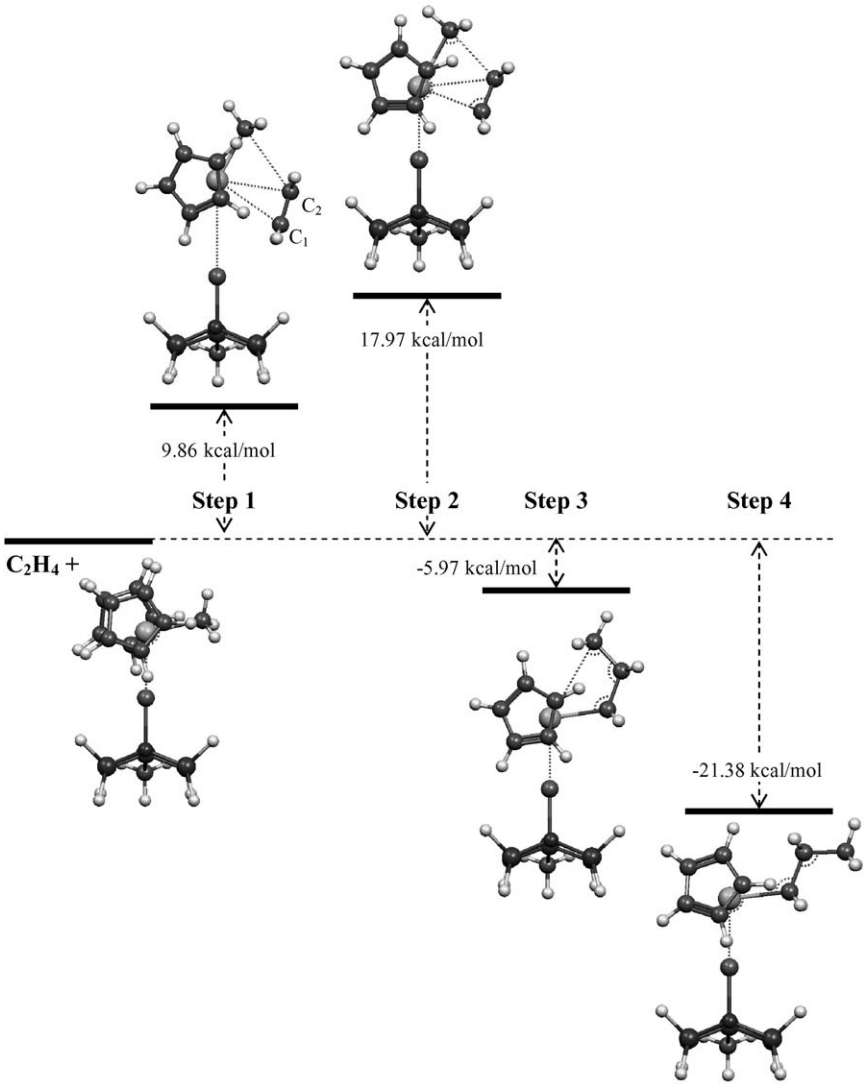

Fig. 4. Energy profile and optimized geometries for the ethylene activation and insertion into the Site 2.

distances when the ethylene molecule is coordinated to the Zr atom in Step 1 were not significantly modified with respect to the isolated species. On the other hand, the cation–anion distance increases noticeably. In all cases, the counterion moves away from the cation to favour the olefin coordination. In the maximum, the four-member state is clearly manifested, with the simultaneous enlargement of the C=C and Zr–C_{CH_3} bonds and the shortening of the Zr–C_1 and Zr–C_2 distances. The monomer presents an asymmetrical coordination with respect to the Zr atom (the Zr–C_1 and Zr–C_2 distances are not equal). At this stage, the counterion is placed closer to the cation than in the previous step. Notice that the cation–anion distance is larger in Site 1 than in Site 2. Therefore, the counterion has a higher steric influence on metallocenic ion, making this part of polymerization process much more difficult in Site 2 than in Site 1. In Step 3, the propyl group is formed by the final ethylene insertion into the Zr–C_{CH_3} bond. The C_1–C_2 and C_2–C_{CH_3} distances are nearly the same. On the other hand, the Zr–C_{CH_3} bond value is very similar to the Zr–C_1 distance found in the initial olefin coordination. Although the propyl group is formed in Step 3, the energy decreases even more than when the alkyl conformer acquires the geometry corresponding to Step 4, where the terminal –CH_3 of propyl locates itself away from the catalytic site. Indeed, in Step 4 the Zr–C_{CH_3} increases noticeably by 4.67 Å. The final geometry of Site 1 is different from that of departure, with a cation–anion distance longer by ∼0.7 Å. On the other hand, the Site 2 acquires a geometric configuration very similar to the initial one. This fact yields a large stabilization of the ionic-pair, as it can be established by the lower ΔE values. All these properties are very similar with or without the presence of the $AlCl_3$ additive.

From the analysis of net atomic and molecular charges, it is possible to understand the electronic changes which take place on the active site during the whole polymerization reaction (see Table 2). The presence of the ethylene molecule in the Zr atom coordination sphere produces charge redistribution in the complete ionic-pair. The magnitudes of the molecular charges of cation and anion increase due to the ethylene insertion (Step 2).

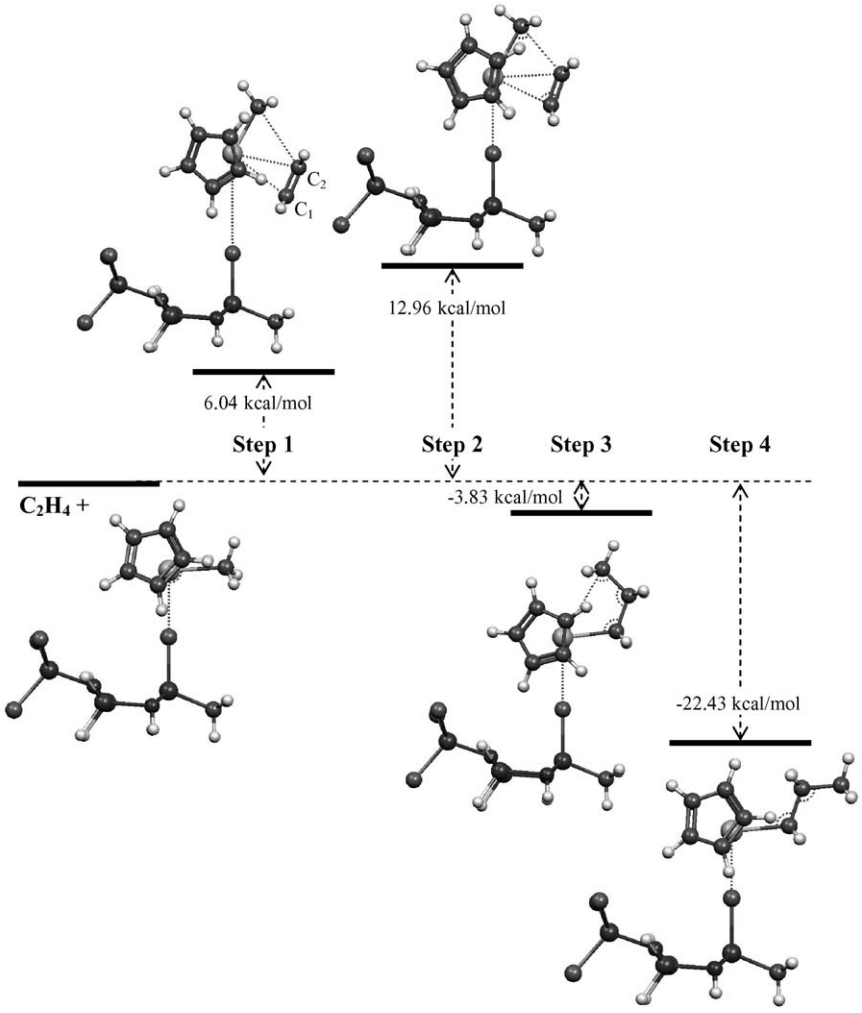

Fig. 5. Energy profile and optimized geometries for the ethylene activation and insertion into the Site 2 with $AlCl_3$.

In the same way, the positive Zr atom charge decreases when the olefin molecule is in this state, indicating an electronic transfer from the ethylene molecule to the Zr atom. The higher decrease is observed for Site 2. Once the propyl group attains its final geometrical configuration in Step 4, the positive Zr atom charge increases and the negative charge of the counterion decreases their magnitude. Site 1 has the Zr atom more positive and the ionic-pair more polarized in comparison with the initial situation (±0.82e and ±0.69e, respectively). However, Site 2 maintains the Zr charge and the initial charge distribution in the ionic-pair. All these observations are the same, independently or not of the presence of the $AlCl_3$ additive.

Finally, the NBO electron transfer energetic parameters between the Zr atom and the olefin in the coordination step and the transition state are summarized in Table 3. The charge transfers parameters from the Zr atom to the antibonding π* molecular orbital of the ethylene increase always at the maximum. This situation is confirmed by the increase of the NBO population of the π* molecular orbital. Indeed, at this stage the π* population increases from 0.015 to 0.204 and from 0.018 to 0.121 for the Sites 1 and 2, respectively. At the same time, we observe that the charge transfer parameters from the bonding π molecular orbital of ethylene to the Zr atom also increase. As a consequence, both factors would contribute to the C_1=C_2 bond rupture. Simultaneously, the σ* population of the Zr–C_{CH_3} bond arises in the TS: it increases from 0.131 to 0.185 and from 0.135 to 0.159 for Sites 1 and 2, respectively. Consequently, the rupture of this bond is also favoured. While these two bonds break (Zr–C_{CH_3} and C_1=C_2) the Zr–C_1 and C_1–C_2 bonds begin to be formed.

If the (π C_2H_4 → Zr) and (Zr → π* C_2H_4), NBO parameters for Step 1 are compared to those for the maximum we observe that the former increase much more than the latter (for example 33.9 kcal/mol versus 16.7 kcal/mol for Site 1). Therefore, it would be expected that at the Step 2 the Zr atom would attain a less positive charge than at Step 1. Moreover, this effect is more noticeably for Site 2 (27.6 kcal/mol versus 6.5 kcal/mol) than for Site 1, predicting an even less positive Zr atom in the first case. A relevant consequence from both observations is that the balance of electronic charge transfers from the olefin to the Zr atom and vice versa is compatible with the Zr NBO atomic charges above commented (see Table 2).

Table 1
Optimized distances obtained for the metallocenic system with ethylene in each step evaluated

Active site		Bond distances (Å)					
		$Zr—C_{CH_3}$ [a]	Zr–O*(Cl) [b]	Zr–C_1 [c]	Zr–C_2 [c]	$C_2—C_{CH_3}$ [a,c]	C_1–C_2 [c]
Site 1	Isolated	2.27	2.95	–	–	–	–
	Step 1	2.28	4.17	2.84	2.89	2.98	1.33
	Step 2	2.34	3.97	2.46	2.73	2.41	1.38
	Step 3	2.83	3.98	2.16	–	1.59	1.57
	Step 4	4.67	3.71	2.26	–	1.56	1.57
Site 1 × $AlCl_3$	Isolated	2.30	2.97	–	–	–	–
	Step 1	2.28	3.94	2.88	2.89	3.00	1.33
	Step 2	2.32	3.89	2.65	2.86	2.79	1.35
	Step 3	2.86	4.02	2.25	–	1.59	1.57
	Step 4	4.70	3.75	2.26	–	1.56	1.57
Site 2	Isolated	2.26	2.58	–	–	–	–
	Step 1	2.28	3.75	3.01	2.88	3.01	1.33
	Step 2	2.48	2.81	2.59	2.93	2.54	1.35
	Step 3	3.44	2.75	2.26	–	1.56	1.60
	Step 4	4.71	2.59	2.27	–	1.56	1.57
Site 2 × $AlCl_3$	Isolated	2.30	2.69	–	–	–	–
	Step 1	2.26	4.23	2.90	2.86	3.09	1.33
	Step 2	2.40	3.15	2.64	2.83	2.58	1.36
	Step 3	3.32	3.02	2.26	–	1.57	1.59
	Step 4	4.68	2.65	2.28	–	1.55	1.56

Parameters calculated using B3LYP hybrid functional with 3-21G**/LanL2DZ basis sets.
[a] The CH_3 as subscript represents the methyl group.
[b] The O* (Cl) is the oxygen atom (chloride atom) which is linked to the Zr atom in Site 1 (Site 2).
[c] The C_1 and C_2 atoms are numbered according to Figs. 2–5.

3.2. Study with two ethylene molecules

For comparison purposes the presence of a second olefin in the proximity of the active site was evaluated. The consideration of the second ethylene in the polymerization reaction was initially proposed by Ystenes in the so-named "trigger mechanism" [27]. According to it, the active site has always a coordinated monomer and a second olefin which helps the first one in the whole polymerization reaction, including both coordination and insertion processes. This proposal was developed to rationalize some experimental data which were not fully explained by the Cossee-Arlman mechanism, i.e., the observation of reaction rate orders higher than 1.0 (1.0–2.0) with respect to the monomer concentration [28].

We studied the coordination plus insertion processes of an ethylene molecule considering the active Site 1 at the presence of a second olefin molecule. In Fig. 6, the geometries of different

Table 2
Molecular and atomic NBO charges for the active site with and without $AlCl_3$, in presence of ethylene molecule

Active site		Species & atoms		
		$Cp_2ZrCH_3^+$	MAO–CH_3Cl^-	Zr
Site 1	Isolated	0.69	−0.69	1.70
	Step 1	0.75	−0.92	1.67
	Step 2	0.82	−0.91	1.58
	Step 4	–	−0.85	1.89
Site 1 × $AlCl_3$	Isolated	0.72	−0.72	1.69
	Step 1	0.74	−0.92	1.66
	Step 2	0.75	−0.91	1.62
	Step 4	–	−0.88	1.89
Site 2	Isolated	0.67	−0.67	1.63
	Step 1	0.71	−0.90	1.62
	Step 2	0.63	−0.74	1.35
	Step 4	–	−0.67	1.61
Site 2 × $AlCl_3$	Isolated	0.73	−0.73	1.69
	Step 1	0.79	−0.96	1.68
	Step 2	0.73	−0.84	1.45
	Step 4	–	−0.71	1.64

Parameters calculated using B3LYP hybrid functional with 3-21G**/LanL2DZ basis sets. Charges are expressed in a.u.

Table 3
NBO electron transfer energetic parameters corresponding of the most relevant molecular orbitals of the system in the first two steps of reaction (in kcal/mol)

Active site		Charge transfers	
		Zr → π* C_2H_4	π C_2H_4 → Zr
Site 1	Step 1	10.48	21.21
	Step 2	27.23	55.11
Site 1 × $AlCl_3$	Step 1	12.56	21.09
	Step 2	25.26	47.27
Site 2	Step 1	4.96	13.69
	Step 2	11.49	41.26
Site 2 × $AlCl_3$	Step 1	11.71	18.51
	Step 2	11.95	36.34

Parameters calculated using B3LYP hybrid functional with 3-21G**/LanL2DZ basis sets.

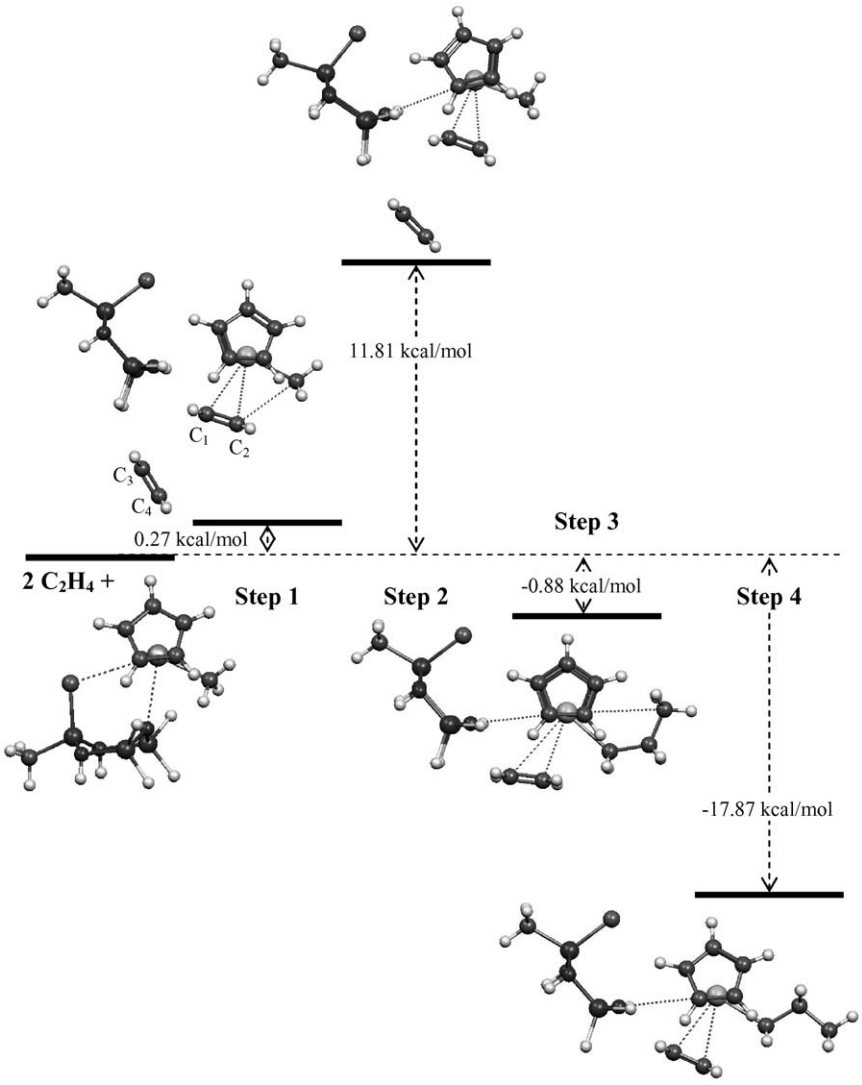

Fig. 6. Energy profile and optimized geometries for the ethylene activation and insertion into the Site 1. In this case a second olefin is triggered by the first one.

steps for the active site with two olefin molecules are shown. The energy profile decreases with respect to that corresponding for the Site 1 with one ethylene molecule. This decrease is much important for Steps 3 and 4 (11.7 and 15.4 kcal/mol, respectively) than for Steps 1 and 2 (6.5 and 2.6 kcal/mol, respectively). Moreover, both Steps 3 and 4 are now exothermic, indicating the high stability for the propyl ionic-pair.

The most relevant geometric parameters for the Site 1 with two monomers are summarized in Table 4. The second olefin was placed initially near the first one, maintaining the C_s symmetry. Then, when the Zr-coordinated complex is formed at Step 1, it moves behind the coordinated olefin. The distance from this molecule to the Zr atom is too large, resulting in a negligible interaction with it. Nevertheless, it is noticeable that the NBO molecular charges of active site and the coordinated olefin is modified by the presence of the second olefin, the first becoming slightly less positive (by 0.09e) and the second slightly positive (by 0.09e). As an indirect consequence, the attractive electrostatic interaction between the two partners of the ionic-pair becomes favoured, decreasing the energy of the system. If

Table 4
Optimized distances obtained for the metallocenic system with two ethylene molecules in each step evaluated

Active site [a]		Bond Distances (Å)				
		Isolated	Step 1	Step 2	Step 3	Step 4
Site 1	Zr—C_{CH_3}	2.27	2.29	2.31	3.94	–
	Zr–O*	2.95	3.88	3.98	3.91	3.98
	Zr–C_1	–	2.92	2.62	2.34	2.32
	Zr–C_2	–	2.83	2.87	–	–
	C_2—C_{CH_3}	–	3.03	2.83	1.56	1.56
	C_1–C_2	–	1.33	1.36	1.61	1.58
	Zr–C_3 [b]	–	6.35	6.31	3.45	2.88
	Zr–C_4 [b]	–	6.82	6.87	2.91	2.89
	C_4–C_1 [b]	–	–	–	2.95	2.99

Parameters calculated using B3LYP hybrid functional with 3-21G**/LanL2DZ basis sets.

[a] See Table 1 for symbols references.

[b] The C_3 and C_4 atoms are numbered according to Fig. 6.

the two olefin molecules compete to coordinate with the Zr atom and the interactions were dominated only by steric effects, the expected influence of the second olefin would be to push the first one towards the Zr atom and to decrease the $Zr–C_1$ and $Zr–C_2$ distances. Nevertheless, this situation was not obtained. In Step 2, the coordinated monomer is near the Zr atom, the position for the second olefin is the same and the counterion remains away from the cation as in Step 1. The Zr-ethylene distance is slightly greater. The geometry of the propyl complex in Site 1 differs markedly in Fig. 6 with respect to Fig. 2. In the Step 3, the propyl geometry is modified due to the presence of the second olefin. The $Zr–C_1$ bond becomes longer than in the case of Fig. 2. The second olefin is now close to the Zr atom, the $Zr–C_3$ distance changing from 6.87 (TS) to 2.91 Å (Step 3). This monomer compels the propyl group to maintain the same orientation as the methyl group. The subsequent restructuring of the new polymer chain gives an additional energetic stability not found in the active site without the other olefin (see Step 4). The second monomer is symmetrically positioned with respect to the Zr atom, in a similar way as it was found the first olefin in Step 1.

Some studies taking into account the influence of a second olefin have been reported. In one case the second olefin molecule attacks into the backside of the cation [29]. This theory could also explain the reaction rate orders between 1.0 and 2.0. Another approach was evaluated by Prosenc et al. [30], which obtained the reaction path for a Cp_2Zr-ethyl isolated cation and two propylene molecules. Nevertheless, in both theoretical analyses the counterion effect was not taken into account.

4. Conclusions

The results presented in this paper show the geometrical, energetic and electronic changes undergone by the coordination and insertion steps of the ethylene molecule in the metallocenic site modelled as ionic-pair. During the predicted polymerization steps, the whole geometry of the active site changes with respect to the isolated situation. The counterion must leave its initial position allowing the olefin to move towards to the Zr atom. The final configuration of Site 1 results in a more polarized ionic-pair with a more opened geometry. Conversely, in the Site 2 the geometry and the charge distribution are preserved. These consequences are reasonable because the Site 1 has a close cation–anion interaction and the Site 2 a comparatively more opened structure. In both cases, the incoming ethylene molecule attains a path to coordinate and insert into the $Zr–C_{CH_3}$ bond. For both active sites, the $AlCl_3$ additive decreases the energetic requirements in all the steps of the process. These observations complement previous theoretical results indicative that this $AlCl_3$ Lewis acid favours energetically the active sites formation.

When two ethylene molecules are present, our calculations indicate that the "trigger" mechanism is thermodynamically more likely than that of one olefin molecule. The energetic requirements are lower for all the analyzed steps. In addition, as postulated by Ystenes, the second olefin forces the formed propyl group to maintain its position and not to flip or reorganize its geometry to achieve an energetically more stable configuration.

Acknowledgement

We would like to thank the financial support from the Consejo Nacional de Investigaciones Científicas y Técnicas (CONICET) and the Universidad Nacional del Sur (UNS) for this research.

References

[1] (a) W. Kaminsky, A. Laban, Appl. Catal. A: Gen. 222 (2001) 47;
(b) N. Suzuki, J. Yu, N. Shioda, H. Asami, T. Nakamura, T. Huhn, A. Fukuoka, M. Ichikawa, M. Saburi, Y. Wakatsuki, Appl. Catal. A: Gen. 224 (2002) 63;
(c) G. Fink, B. Steinmetz, J. Zechlin, Ch. Przybyla, B. Tesche, Chem. Rev. 100 (2000) 1377;
(d) J.N. Pédeutour, K. Radhakrishnan, H. Cramail, A. Deffieux, J. Mol. Catal. A: Chem. 185 (2002) 119;
(e) G. Di Silvestro, A. Galbiati, Y.C. Minga, N. Caronzolo, E. Cesarotti, J. Mol. Catal. A: Chem. 204–205 (2003) 315;
(f) E. Zurek, T. Ziegler, Organometallics 21 (2002) 83;
(g) N.I. Mäkelä-Vaarne, M. Linnolahti, T.A. Pakkanen, M.A. Leskelä, Macromolecules 36 (2003) 3854.
[2] Y.-X. Chen, C.L. Stern, T.J. Marks, J. Am. Chem. Soc. 119 (1997) 2582, and references therein.
[3] F. Grisi, P. Longo, A. Zambelli, J.A. Ewen, J. Mol. Catal. A: Chem. 140 (1999) 225.
[4] V.L. Cruz, A. Muñoz-Escalona, J. Martinez-Salazar, J. Polym. Sci: Part A. Polym. Chem. 36 (1998) 1157.
[5] S. Martinez, V. Cruz, A. Muñoz-Escalona, J. Martinez-Salazar, Polymer 44 (2003) 295.
[6] G. Lanza, I.L. Fragalà, T.J. Marks, J. Am. Chem. Soc. 120 (1998) 8257.
[7] M.S.W. Chan, K. Vanka, C.C. Pye, T. Ziegler, Organometallics 18 (1999) 4624.
[8] E. Zurek, T. Ziegler, Faraday Discuss. 124 (2003) 93.
[9] H. Weiss, M. Ehrig, R. Ahlrichs, J. Am. Chem. Soc. 116 (1994) 4919.
[10] T.K. Woo, L. Fan, T. Ziegler, in: Fink, Mülhaupt, Brintzinger (Eds.), Ziegler Catalysts, Springer-Verlag, Berlin, 1995, p. 291.
[11] K. Thorshaug, J.A. Støvneng, E. Rytter, M. Ystenes, Macromolecules 31 (1998) 7149.
[12] P.G. Belelli, M.M. Branda, N.J. Castellani, J. Mol. Catal. A: Chem. 192 (1–2) (2003) 9.
[13] M. Ystenes, J.L. Eilertsen, J. Liu, M. Ott, E. Rytter, J.A. Støvneng, J. Polym. Sci. Part A: Polym. Chem. 38 (2000) 3106.
[14] P.G. Belelli, D.E. Damiani, N.J. Castellani, J. Mol. Catal. A: Chem. 208 (2004) 147.
[15] (a) P. Cossee, J. Catal. 3 (1964) 80;
(b) E.J. Arlman, P. Cossee, J. Catal. 3 (1964) 99;
(c) L.A. Castonguay, A.K. Rappé, J. Am. Chem. Soc. 114 (1992) 5832;
(d) E.P. Bierwagen, J.E. Bercaw, W.A. Goddard, J. Am. Chem. Soc. 116 (1994) 1481;
(e) N. Koga, T. Yoshida, K. Morokuma, in: G. Fink, R. Mülhaupt, H.H. Brintzinguer (Eds.), Ziegler Catalysts, Springer, Berlin, 1995, p. 275;
(f) T.K. Woo, P.M. Margl, J.C.W. Lohrenz, P.E. Blöchl, T. Ziegler, J. Am. Chem. Soc. 118 (1996) 13021.
[16] W. Kohn, L. Sham, Phys. Rev. 140 (1965) A1133.
[17] R.G. Parr, W. Yang, Density-functional Theory of Atoms and Molecules, Oxford University Press, Oxford, 1989.
[18] (a) P.J. Hay, W.R. Wadt, J. Chem. Phys. 82 (1985) 270;
(b) W.R. Wadt, P.J. Hay, J. Chem. Phys. 82 (1985) 284;
(c) P.J. Hay, W.R. Wadt, J. Chem. Phys. 82 (1985) 299.
[19] (a) V.L. Cruz, A. Muñoz-Escalona, J. Martinez-Salazar, Polymer 37 (1996) 1663;
(b) L. Petitjean, D. Pattou, M.F. Ruiz-López, J. Phys. Chem. B 103 (1999) 27.

[20] M.J. Frisch, y col., Gaussian 03, Revision C.02, Gaussian Inc., Pittsburgh, PA, 2003.
[21] (a) A.E. Reed, L.A. Curtiss, F. Weinhold, Chem. Rev. 88 (1988);
(b) E.D. Glendening, A.E. Reed, J.E. Carpenter, F. Weinhold, NBO Version 3.1 in Gaussian 03 (see Ref. [20]).
[22] (a) H.B. Schlegel, J. Comp. Chem. 3 (1982) 214;
(b) H.B. Schlegel, in: J. Bertran (Ed.), New Theoretical Concepts for Understanding Organic Reactions, Kluwer Academic, The Netherlands, 1989, pp. 33–53.
[23] (a) M.S.W. Chan, T. Ziegler, Organometallics 19 (2000) 5182;
(b) E. Zurek, T. Ziegler, Prog. Polym. Sci. 29 (2004) 107.
[24] P.G. Belelli, D.E. Damiani, N.J. Castellani, Chem. Phys. Lett. 401 (2005) 515.
[25] P.G. Belelli, M.L. Ferreira, D. Damiani, Macromol. Chem. Phys. 201 (2000) 1458.
[26] P.G. Belelli, M.L. Ferreira, D.E. Damiani, Stud. Suf. Sci. Catal. 130 (2000) 3855.
[27] M. Ystenes, J. Catal. 129 (1991) 383.
[28] (a) T. Keii, K. Soga, N. Saiki, J. Polym. Sci. Polym. Symp. 16 (1967) 1507;
(b) N. Herfert, G. Fink, Macromol. Chem. 193 (1992) 1359;
(c) M. Ystenes, Makromol. Chem. Macromol. Symp. 66 (1993) 71;
(d) Z. Yu, J.C.W. Chien, J. Polym. Sci. A 33 (1995) 125;
(e) J.C.W. Chien, Z. Yu, M.M. Marques, J.C. Flores, M.D. Rausch, J. Polym. Sci. Part A: Polym. Chem. 36 (1998) 319.
[29] A. Muñoz-Escalona, J. Ramos, V. Cruz, J. Martínez-Salazar, J. Poym. Sci: Part A: Polym. Chem. 38 (2000) 571.
[30] M.H. Prosenc, F. Schaper, H.H. Brintzinger, in: W. Kaminsky (Ed.), Metallorganic Catalyst for Synthesis and Polymerization, Springer-Verlag, Berlin, Heidelberg, 1999, p. 223.